

MEASURING NEUTRON STAR RADII VIA PULSE PROFILE MODELING WITH NICER

FERYAL ÖZEL¹, DIMITRIOS PSALTIS¹, ZAVEN ARZOUMANIAN², SHARON MORSINK³, AND MICHI BAUBÖCK¹

Draft version March 3, 2024

ABSTRACT

The Neutron-star Interior Composition Explorer (NICER) is an X-ray astrophysics payload that will be placed on the International Space Station. Its primary science goal is to measure with high accuracy the pulse profiles that arise from the non-uniform thermal surface emission of rotation-powered pulsars. Modeling general relativistic effects on the profiles will lead to measuring the radii of these neutron stars and to constraining their equation of state. Achieving this goal will depend, among other things, on accurate knowledge of the source, sky, and instrument backgrounds. We use here simple analytic estimates to quantify the level at which these backgrounds need to be known in order for the upcoming measurements to provide significant constraints on the properties of neutron stars. We show that, even in the minimal-information scenario, knowledge of the background at a few percent level for a background-to-source count-rate ratio of 0.2 allows for a measurement of the neutron star compactness to better than 10% uncertainty for most of the parameter space. These constraints improve further when more realistic assumptions are made about the neutron star emission and spin, and when additional information about the source itself, such as its mass or distance, are incorporated.

Subject headings: stars: neutron — dense matter — equation of state — pulsars: general — gravitation

1. INTRODUCTION

Periodic brightness oscillations originating from the surface of a neutron star provide a powerful means of measuring its mass and radius (see Strohmayer 2004 for an early review). In the case of rotation-powered pulsars, the temperature non-uniformity that causes the brightness oscillations is due to the magnetic field topology of the stellar surface and the associated energetic particle flux from the magnetosphere, which heats the polar caps relative to the rest of the star such that they emit in the soft X-ray band (e.g., Ruderman & Sutherland 1975; Arons 1981; Harding & Muslimov 2001, 2002; Bai & Spitkovsky 2010a, b). The trajectories of the photons emitted from the surface are bent by the strong gravitational field of the neutron star, imparting on the pulse shapes and amplitudes information about the stellar compactness (e.g., Pechenick et al. 1983; Weinberg et al. 2001; Poutanen & Beloborodov 2006; Cadeau et al. 2007; Psaltis & Özel 2014).

The degree to which this information can be decoded to infer the mass and radius, either jointly or separately, depends on a number of factors such as the X-ray brightness of the neutron star, its spin period, P , the beaming pattern of the radiation emitted from the surface, as well as the spot colatitude θ_s and the inclination of the observer i with respect to the stellar spin axis. This is because all of these variables, along with the stellar compactness, determine the pulse amplitude and its shape (i.e., the amplitudes of the harmonics). In addition, there are several sources of background that affect the measurement of the properties of the pulse profiles, such as X-ray emission from the magnetosphere or the rest of the neutron star surface, X-ray emission from other sources in the field of view, and instrumental background. The resulting signal-to-background ratio ultimately determines the accuracy with which the stellar compactness, $u = 2GM/Rc^2$, can be measured for a star of mass M and radius R .

NICER is a NASA mission, currently in development, designed primarily to observe thermal X-rays originating from the polar caps of a number of rotation-powered millisecond pulsars. Its goal is to analyze pulse profiles to measure the stellar compactness and radius (Gendreau et al. 2012; Arzoumanian et al. 2014). Being a dedicated mission, it will have the ability to observe selected sources for long periods to accumulate the necessary number of counts to measure the properties of the pulse profile. Nevertheless, the accuracy it will achieve in the measurement of the various harmonic amplitudes, and, thus, in the compactness, will depend on the level and our knowledge of the several sources of background. Because it is not an imaging instrument and because of the International Space Station environment, it will register both time-varying and constant sources of background, arising from the various origins discussed above. In this paper, we formulate the effect of the background on the pulse profiles and investigate the background tolerances that will still enable 5-10% accuracy in the measurements of the neutron star properties, which is necessary to pin down the dense matter equation of state. We provide approximate formulae for the uncertainties in the inferred stellar compactness and radius as a function of the signal-to-noise ratio, the uncertainty in the measurement of the background, and the uncertainty in the system geometry, described by the spot colatitude and the observer's inclination.

Thermal emission from the polar caps of rotation powered pulsars has been observed with previous generations of X-ray satellites (Ögelman 1991; Finley et al. 1992; Becker & Trümper 1993; Pavlov & Zavlin 1997). Pulsed X-ray

¹ Astronomy Department, University of Arizona, 933 N. Cherry Ave., Tucson, AZ 85721, USA; fozel@email.arizona.edu

² Center for Research and Exploration in Space Science and Technology & X-Ray Astrophysics Laboratory, NASA Goddard Space Flight Center, Code 662, Greenbelt, MD 20771, USA

³ Department of Physics, University of Alberta, 11455 Saskatchewan Drive, Edmonton, AB T6G 2E1, Canada

emission has been detected and the thermal X-ray brightness has been determined for a number of sources, such as PSR J0437–4715, PSR J0030+0451, PSR J2124–3358, and PSR J1024–0719, most recently by targeted Chandra and XMM-Newton observations (e.g., Zavlin 2006; Bogdanov et al. 2007; Bogdanov & Grindlay 2009; Bogdanov 2013). In addition, the number of rotation-powered millisecond pulsars has grown exponentially in recent years, thanks to discoveries by the *Fermi* satellite (e.g., Abdo et al. 2013) and radio surveys⁴, some of which are likely to exhibit pulsed soft X-ray emission. The spectra are usually described by a thermal component originating from the surface, typically modeled by unmagnetized hydrogen atmospheres or blackbodies, as well as a non-thermal component, likely of magnetospheric origin, which manifests itself as a power-law tail at higher energies. Using this pulsed surface emission to constrain the neutron star properties has so far led to broad constraints on masses and radii (Zavlin 2006; Bogdanov et al. 2007; Bogdanov & Grindlay 2009; Bogdanov 2013).

The rotation-powered pulsars that are the primary targets for NICER have spin frequencies of 200 – 400 Hz. This range of relatively low frequencies (compared to neutron stars in some accreting systems) minimizes higher order spin effects such as the stellar oblateness and the spacetime quadrupole (Morsink et al. 2007; Cadeau et al. 2007; Psaltis & Özel 2014; Psaltis et al. 2014). The first order Doppler effects can still be appreciable in this range of spin frequencies. This simplifies the modeling by allowing us to treat the stellar spacetime in the Schwarzschild+Doppler approximation. A large amount of work has been carried out in this regime, starting with the numerical calculations of self-lensing in the Schwarzschild metric by Pechenick et al. (1983) and its application to the millisecond brightness oscillations observed by the Rossi X-ray Timing Explorer (Strohmayer et al. 1997; Nath et al. 2002). Furthermore, Poutanen & Beloborodov (2006) devised an analytic expression that we use in the present study when calculating the amplitudes of the harmonics.

In this paper, we investigate the effect of background on the determination of the neutron star compactness given measurements of the shapes of pulse profiles from rotation-powered pulsars. Specifically, we make use of the analytic formulae for the pulse shapes of moderately spinning neutron stars in the Schwarzschild metric to calculate the number of observables one can determine from the profiles in different situations. We then use these to quantify the level at which the various sources of background must be independently known in order for the upcoming NICER measurements to provide significant constraints on the properties of neutron stars.

2. MEASURING THE PROPERTIES OF PULSE PROFILES

In the following, we will assume that the surface emission of a slowly spinning, rotation powered pulsar originates in one small circular polar cap on its surface. Bauböck et al. (2015) estimated the typical sizes of polar caps, defined as the radius within which the open magnetic field lines originate from the neutron star surface, for the NICER targets. The analytic estimates in that study of the size of the polar cap (Bauböck et al. 2015), as well as numerical simulations of surface heating caused by return magnetospheric currents (e.g., Bai & Spitkovsky 2010), support the assumption that the polar cap size is too small for its detailed emission structure to affect the pulse profile observed at infinity. Because of this, we make the small spot approximation when calculating the harmonic amplitudes of the pulse profiles. However, observations of the prototypical NICER target, PSR J0437–4715, suggest that its surface emission may arise from two small but non-antipodal polar caps (Bogdanov 2014). This latter case is more complicated than what we explore here and will change the actual shape of the pulse profile, but its complexity does not severely affect our conclusions in the uncertainties achieved in the various quantities as a function of count rate and backgrounds.

For a slowly spinning neutron star, the pulse profile observed by NICER will be characterized by the following quantities (see Figure 1): the background countrate A , the constant component of the pulse profile Q , the amplitudes V_n and the phases ϕ_n of the various harmonics, and, if present, the phase ϕ_p beyond which the flux from the polar cap is blocked by the star. The general form of the profile will be

$$F(t) = A + \begin{cases} Q + \sum_{n=1} V_n \cos\left(\frac{2\pi nt}{P} + \phi_n\right), & \text{if } |2\pi t/P| < \phi_p \\ 0, & \text{otherwise} \end{cases} \quad (1)$$

If the spin of the neutron star is significant, then additional harmonics appear in the profile with orthogonal phases.

The total number of counts collected when N periods are accumulated is equal to

$$\begin{aligned} C &= N \int_0^P F(t) dt \\ &= \left(A + Q \frac{\phi_p}{\pi}\right) NP + 2N \sum_{n=1} V_n \int_0^{P\phi_p/2\pi} \cos\left(\frac{2\pi nt}{P} + \phi_n\right) dt \\ &= \left(A + Q \frac{\phi_p}{\pi}\right) NP + \sum_{n=1} \frac{V_n NP}{\pi} [\sin(n\phi_p + \phi_n) - \sin \phi_n] . \end{aligned} \quad (2)$$

The uncertainty in the measurement of the total number of counts will simply be

$$\sigma_C = \sqrt{C} \simeq \sqrt{(A + Q)NP} , \quad (3)$$

⁴ See <https://confluence.slac.stanford.edu/display/GLAMCOG/Public+List+of+LAT-Detected+Gamma-Ray+Pulsars> and <http://astro.phys.wvu.edu/GalacticMSPs> for up-to-date lists.

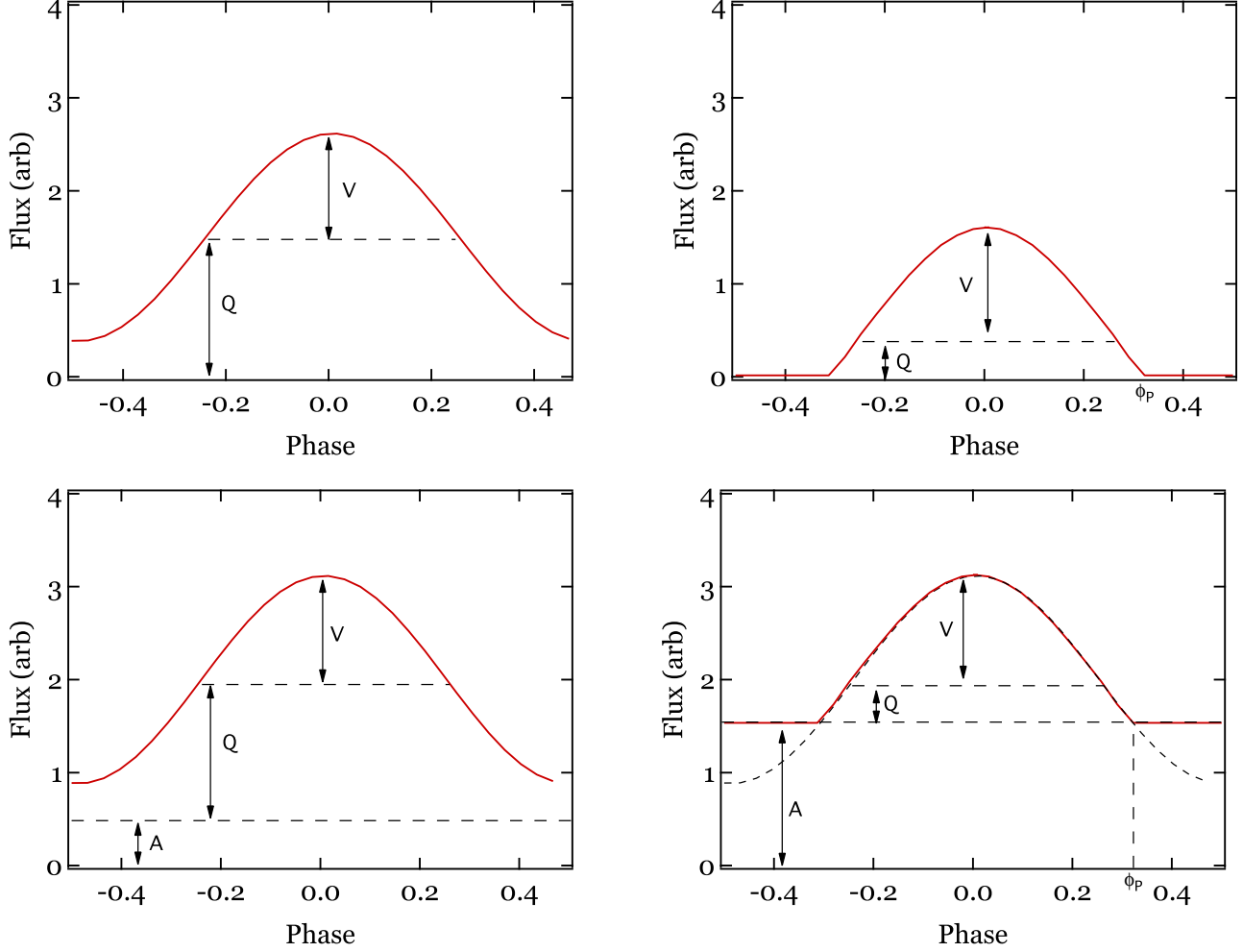


FIG. 1.— Pulse profiles generated by a circular hot spot on the surface of a slowly spinning neutron star, without (*top*) and with (*bottom*) instrument or sky background. The left panels show a situation in which the polar cap is visible throughout the pulse period, whereas the right panels show the pulse shape when the polar cap is hidden behind the star for part of the period. In general, a profile is characterized by four quantities: the constant component of the pulse profile Q (see Eq. 1), the amplitude of the sinusoidal profile V (assumed for the purposes of this figure to have only a non-zero fundamental component), the background count rate A , and, potentially, the phase ϕ_p beyond which the polar cap is not visible to the observer. Note that pulse phase in the interval $[-0.5 - 0.5]$ is shown here, but radians are used in the equations and text.

where, in the last equality, we assumed that the polar cap is visible throughout the pulse period (i.e., $\phi_p = \pi$). From this last equation, we also get the uncertainty in measuring the sum $Q + A$ as

$$\sigma_{Q+A} = \frac{\sigma_c}{NP} = \sqrt{\frac{A+Q}{NP}}. \quad (4)$$

In the following calculation, we will need primarily the constant component of the source count rate Q and the associated uncertainty σ_Q . In order to do this, we will need a measurement of the background count rate, A , and its associated uncertainty, σ_A . The latter will have a Poisson component that will depend on the total time T used to measure the background, as well as a possible systematic component, such as

$$\sigma_A = \sqrt{\frac{A}{T}} + \lambda A \quad (5)$$

with λ an appropriate constant. With these definitions, we obtain

$$\begin{aligned} \frac{\sigma_Q}{Q} &= \frac{(\sigma_{Q+A}^2 + \sigma_A^2)^{1/2}}{Q} \\ &= \left[\left(\frac{A}{Q} + 1 \right) \frac{1}{QNP} + \left(\frac{\sigma_A}{A} \right)^2 \left(\frac{A}{Q} \right)^2 \right]^{1/2}. \end{aligned} \quad (6)$$

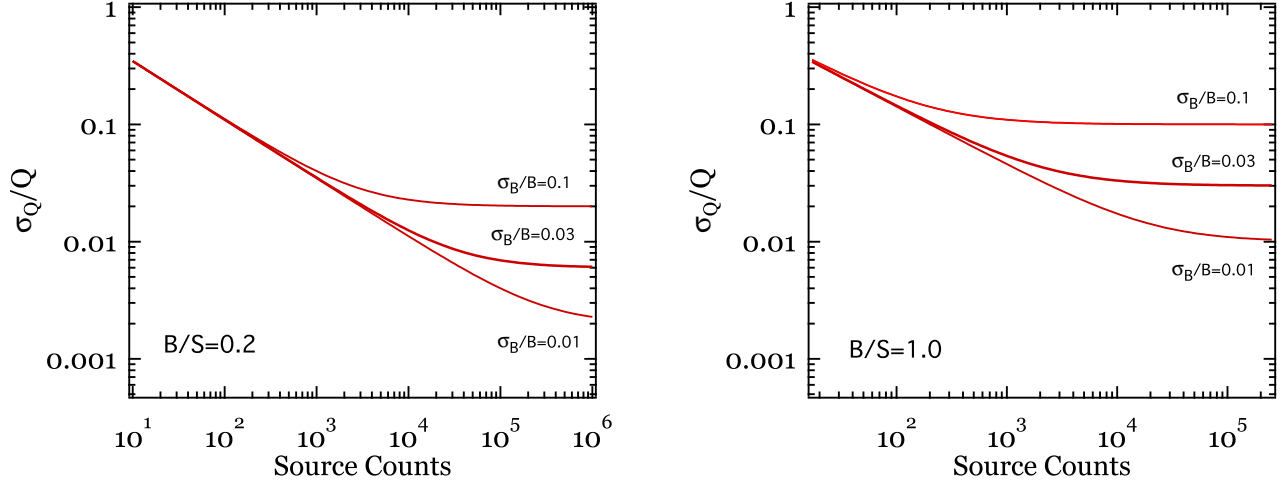


FIG. 2.— Predicted fractional uncertainties in the measurement of the quantity Q , i.e., the constant component, for a nearly sinusoidal pulse profile, as a function of the total number of source counts collected. The two panels correspond to two different ratios of the background to source counts and different curves in each panel are labeled by the fractional uncertainty in the knowledge of the background counts σ_B/B .

We can also write this equation in terms of the total source counts $S = QNP$ and the total background counts $B = ANP$ as

$$\frac{\sigma_Q}{Q} = \left[\left(\frac{B}{S} + 1 \right) \frac{1}{S} + \left(\frac{\sigma_B}{B} \right)^2 \left(\frac{B}{S} \right)^2 \right]^{1/2}. \quad (7)$$

Figure 2 shows the predicted fractional uncertainties in the measurement of the quantity Q as a function of the total number of source counts collected. In making this figure, we have assumed a constant fractional uncertainty in the *a priori* knowledge of the background, i.e., σ_B/B , and a constant ratio of background to source counts, i.e., B/S . Under these assumptions, the asymptotic value of the uncertainty (i.e., for a large number of source counts) is dominated by the uncertainty in the knowledge of the background and scales as

$$\lim_{S \rightarrow \infty} \frac{\sigma_Q}{Q} = \left(\frac{\sigma_B}{B} \right) \left(\frac{B}{S} \right). \quad (8)$$

In other words, the fractional uncertainty in the measurement of Q is limited by the product of the fractional uncertainty in the knowledge of the background times the ratio of the background to source counts.

The additional quantities that we can measure from the pulse profile are the fractional r.m.s. amplitudes of the various harmonics. Considering, for example, the n -th harmonic, the measured fractional r.m.s. amplitude (including the background) is

$$r_{\text{obs}} = \frac{V_n}{\sqrt{2}(Q+A)}. \quad (9)$$

Using the result in Psaltis et al. (2014), the uncertainty in the measurement of r_{obs} scales as

$$\sigma_{r,\text{obs}} = \frac{\sqrt{S+B}}{S} = \frac{\sqrt{(A+Q)NP}}{QNP}, \quad (10)$$

from which we can write

$$\begin{aligned} \sigma_V^2 &= \left(\frac{\partial V_n}{\partial r_{\text{obs}}} \right)^2 \sigma_{r,\text{obs}}^2 + \left[\frac{\partial V_n}{\partial (Q+A)} \right]^2 \sigma_{Q+A}^2 \\ &= \frac{2(Q+A)^3}{Q^2 NP} + \frac{V_n^2}{(Q+A)NP}. \end{aligned} \quad (11)$$

The fractional uncertainty in the measurement of the amplitude is

$$\frac{\sigma_V}{V_n} = \left[2 \left(1 + \frac{A}{Q} \right)^3 \left(\frac{Q}{V_n} \right)^2 \frac{1}{QNP} + \left(1 + \frac{A}{Q} \right)^{-1} \frac{1}{QNP} \right]^{1/2}. \quad (12)$$

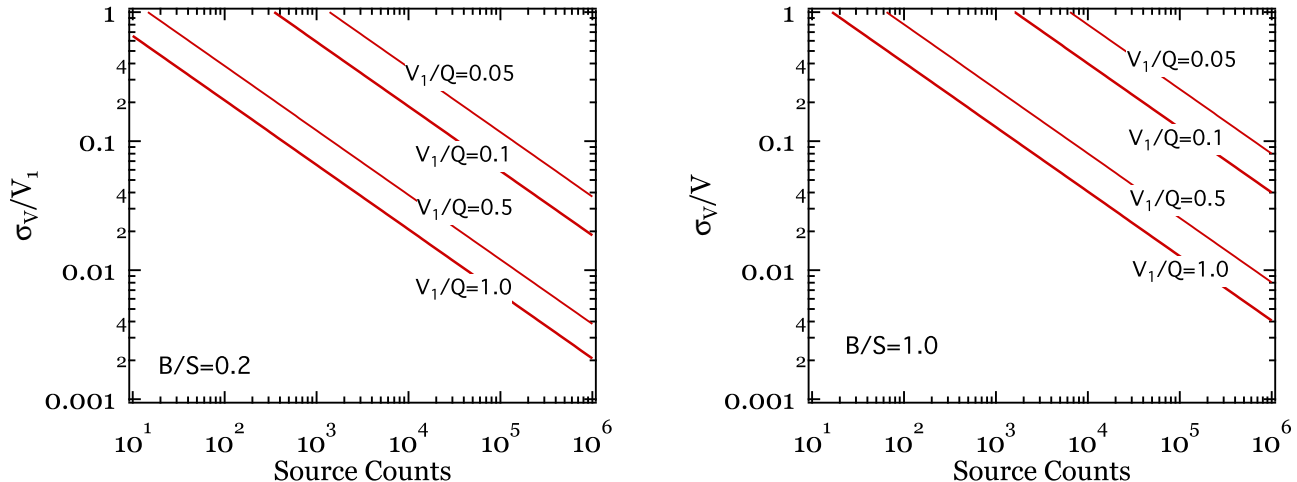


FIG. 3.— Predicted fractional uncertainties in the measurement of the quantity V_1 , i.e., the amplitude of the fundamental, for a nearly sinusoidal pulse profile, as a function of the total number of source counts collected. The two panels correspond to different ratios of the background to source counts and different curves in each panel are labeled by the intrinsic fractional amplitude of the pulsations V_1/Q .

Writing this equation in terms of the total number of source and background counts, we obtain

$$\frac{\sigma_V}{V_n} = \left[2 \left(1 + \frac{B}{S} \right)^3 \left(\frac{Q}{V_n} \right)^2 + \left(1 + \frac{B}{S} \right)^{-1} \right]^{1/2} \frac{1}{S^{1/2}}. \quad (13)$$

Figure 3 shows the predicted fractional uncertainty in the measurement of the quantity V , as a function of the total number of source counts. As the last equation shows, the uncertainty in the measured amplitude of pulsations simply scales as the inverse square root of the source counts.

Finally, the last quantity to be measured, when present in the pulse profile, is the phase ϕ_P , beyond which the polar cap is blocked by the star. The main uncertainty in this measurement will arise from the fact that the evolution of the pulse profile with phase is masked by the uncertainty in the background, i.e.,

$$V_1 \cos(\phi_P + \delta\phi_P) \simeq \sigma_A. \quad (14)$$

Setting $\sigma_\phi \equiv \delta\phi_P$, we can use this equation to find

$$\sigma_\phi = \frac{\sigma_A}{V_1 \sin \phi_P}. \quad (15)$$

and write this last equation in the more useful form

$$\sigma_\phi = \frac{1}{\sin \phi_P} \left(\frac{\sigma_B}{B} \right) \left(\frac{B}{S} \right) \left(\frac{Q}{V_1} \right). \quad (16)$$

For the remainder of our discussion, we will only consider pulse shapes in which the polar cap is visible throughout the pulse period.

3. FROM PULSE PROFILES TO STELLAR COMPACTNESS

Having measured the characteristic properties of a pulse profile, i.e., its constant component Q and the amplitudes V_n and phases ϕ_n of its various harmonics, we can use theoretical models of the gravitationally lensed emission from a neutron-star hotspot to obtain the compactness and the radius of the neutron star.

In the following, we will make use of the approximate analytic expressions and terminology of Poutanen & Beloborodov (2006). These expressions take into account light bending around a slowly spinning star and yield the bolometric flux observed at infinity under the assumption that the polar cap is infinitesimally small and that no emission emerges from the rest of the star. We will denote by M and R the mass and radius of the neutron star, by P its spin period, by i the inclination of the observer with respect to the spin axis, and by θ the colatitude of the hot spot.

Model atmospheres of neutron stars, in general, and of magnetic polar caps, in particular, show that the emission from the neutron-star surface is not isotropic but is beamed (see, e.g., the discussion in Özel 2013). We will represent this beaming with a functional form

$$I(\alpha) = I_0(1 + h \cos \alpha), \quad (17)$$

where α is the emission angle with respect to the normal to the surface and h is a quantity that is calculated from model atmospheres and measures the degree of beaming ($h = 0$ being the isotropic limit).

We will also define the compactness of the neutron star as

$$u \equiv \frac{2GM}{Rc^2} \quad (18)$$

as well as the following two quantities

$$\begin{aligned} q &\equiv u + (1 - u) \cos i \cos \theta \\ v &\equiv (1 - u) \sin i \sin \theta . \end{aligned} \quad (19)$$

The relations between the characteristics of the pulse profile (see eq. [1]) and the properties of a slowly spinning neutron star are (Poutanen & Beloborodov 2006, eq. [28]-[38])

$$\begin{aligned} Q &= I_0 \mathcal{G} \frac{dS}{D^2} \left[q + h \left(q^2 + \frac{v^2}{2} \right) \right] \\ V_1 &= I_0 \mathcal{G} \frac{dS}{D^2} \frac{(1 + 2hq)v}{\cos \phi_1} \\ V_2 &= I_0 \mathcal{G} \frac{dS}{D^2} \frac{hv^2}{2 \cos \phi_2} \\ \tan \phi_1 &= \frac{(3 + \Gamma)q + (4 + \Gamma)h(q^2 + v^2/4)}{u(1 + 2hq)} \left(\frac{2\pi R}{cP} \right) \sin i \sin \theta \\ \tan \phi_2 &= \frac{(4 + \Gamma)(1 + 2hq) - 1}{hu} \left(\frac{2\pi R}{cP} \right) \sin i \sin \theta . \end{aligned} \quad (20)$$

In these equations, dS is the surface area of the polar cap, D is the distance to the source, Γ is the photon index of the spectrum, and \mathcal{G} is a (calculable) factor that depends on the spectrum of the source and the photon-energy range of the detector.

3.1. The Limiting Case of Minimal Information

To calculate the background tolerances in the measurements of the neutron star properties from the characteristics of its pulse profile, we will first consider the worst possible case, i.e., one in which the emission from the neutron star surface is isotropic and the Doppler effects on the pulse profile are not measurable. Although this is not expected in reality, this situation both reduces the amplitude of the fundamental (exacerbating background effects) and the amplitudes of the harmonics, thus minimizing the number of measurable quantities in the profile. This can be seen by taking the limit $h = 0$ and $2\pi R/cP \rightarrow 0$ in the above equations, which simplifies them to

$$\begin{aligned} Q &= I_0 \mathcal{G} \frac{dS}{D^2} q \\ V_1 &= I_0 \mathcal{G} \frac{dS}{D^2} v \\ V_2 &= 0 . \end{aligned} \quad (21)$$

One of the most significant benefits of neutron-star radius measurements with pulse profile modeling is that, in principle, they can provide results that are independent of any prior knowledge of the distance to each source (although, as we will discuss below, when precise distance measurements are available, they can be folded in to increase the number of independently measured quantities from the pulse profile). In order not to rely on the distance information, we cannot separately use the absolute constant component and fundamental amplitude of the pulse profile (both of which depend on the size of the polar cap and on the distance), but we can only consider the fractional amplitude of the fundamental, i.e.,

$$r_1 \equiv \frac{V_1}{Q} = \frac{v}{q} = \frac{(1 - u) \sin i \sin \theta}{u + (1 - u) \cos i \cos \theta} . \quad (22)$$

In this last step, we used the definitions (19) to connect the pulse profile properties to the neutron-star compactness. Solving this last equation for the compactness u , we obtain

$$u = \frac{r_1 \cos i \cos \theta - \sin i \sin \theta}{-r_1 + r_1 \cos i \cos \theta - \sin i \sin \theta} . \quad (23)$$

Clearly, in order to measure the neutron-star compactness in this case, we need independent knowledge of the inclination of the observer, i , and of the colatitude of the polar cap, θ . Such prior knowledge is not unreasonable for many rotation-powered pulsars, the geometries of which can be inferred by fitting model γ -ray pulse profiles to *Fermi* observations of individual sources (Johnson et al. 2014) and, to a certain extent, by modeling polarization angle swings in the radio (Yan et al. 2011; Dai et al. 2015).

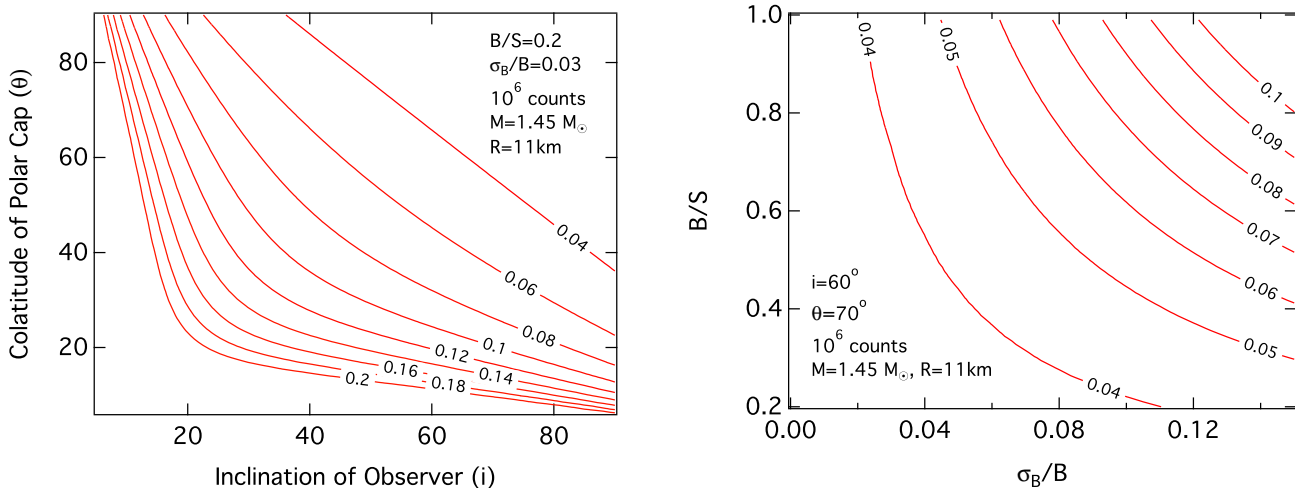


FIG. 4.— (Left) Contours of constant predicted fractional error in the measurement of a neutron-star compactness u , for different orientations of the observer i and colatitudes of the polar cap θ . For this set of calculations, we assumed a neutron star mass of $1.45 M_{\odot}$ and a radius of 11 km, as well as a total of 10^6 source counts, a background-to-source count ratio $B/S = 0.2$, and an uncertainty in the background $\sigma_B/B = 0.03$. We also assumed that the two angles i and θ to be known with an uncertainty of $\sigma_i = \sigma_{\theta} = 2^{\circ}$. (Right) Contours of constant predicted fractional error in the measurement of a neutron-star compactness u , for different background-to-source count ratios B/S and amount of uncertainty in the background σ_B/B . For this set of calculations, the inclination of the observer was set to $i = 60^{\circ}$ and the colatitude of the polar cap was set to $\theta = 70^{\circ}$. The remaining parameters are the same as in the left panel.

The uncertainty within which the fractional amplitude of the fundamental can be measured is

$$\frac{\sigma_{r1}}{r_1} = \left(\frac{\sigma_{V1}^2}{V_1^2} + \frac{\sigma_Q^2}{Q^2} \right)^{1/2}, \quad (24)$$

where σ_Q/Q and σ_{V1}/V_1 are given by equations (7) and (13), respectively. At the limit of a very large number of counts,

$$\lim_{S \rightarrow \infty} \frac{\sigma_{r1}}{r_1} = \left(\frac{\sigma_B}{B} \right) \left(\frac{B}{S} \right). \quad (25)$$

Using these expressions, we can finally write the uncertainty in the measurement of the neutron-star compactness as

$$\begin{aligned} \sigma_u &= \left[\left(\frac{\partial u}{\partial r_1} \right)^2 \sigma_{r1}^2 + \left(\frac{\partial u}{\partial i} \right)^2 \sigma_i^2 + \left(\frac{\partial u}{\partial \theta} \right)^2 \sigma_{\theta}^2 \right]^{1/2} \\ &= \left[\sigma_{r1}^2 \sin^2 i \sin^2 \theta + \frac{1}{2} r_1^3 \sin(2i) \sin(2\theta) (\sigma_i^2 + \sigma_{\theta}^2) \right. \\ &\quad \left. + r_1^2 \cos^2 i \sin^2 \theta (\sigma_i^2 + r_1^2 \sigma_{\theta}^2) \right. \\ &\quad \left. + r_1^2 \sin^2 i \cos^2 \theta (r_1^2 \sigma_i^2 + \sigma_{\theta}^2) \right]^{1/2} \\ &\quad (r_1 - r_1 \cos i \cos \theta + \sin i \sin \theta)^{-2}. \end{aligned} \quad (26)$$

Here, σ_i and σ_{θ} are the uncertainties (in radians) in the prior knowledge of the observer inclination and of the colatitude of the polar cap.

Figure 4 shows the predicted fractional uncertainties in the measurement of the compactness of a neutron star, for different parameters of the system as well as for different degrees of knowledge of the background to the source. When the geometric angles i and θ are reasonably well known via other measurements, these figures show that knowledge of the background at a few percent level allows a measurement of the neutron star compactness to better than 10% uncertainty for most of the parameter space. This result is obtained for a background-to-source ratio of 0.2, which is achievable for the brightest NICER targets, and a total accumulation of 10^6 counts. It is only when the pulse amplitudes plummet for the cases where either the observer or the polar cap are nearly aligned with the spin axis that the uncertainties become larger than 15% (see the left panel of Fig. 4). When the system geometry is such that the pulse amplitudes are reasonably large (as is the case with prototypical NICER targets), the right panel of Figure 4 shows the dependence of the fractional error in the neutron star compactness for different background-to-signal ratios and different levels of uncertainty in the determination of the background. Even when the background is comparable to the signal and is measured only to within $\approx 15\%$, the fractional error in the compactness remains at or below 10%. Note that this is for the minimal-information case of isotropic beaming, where only one fractional amplitude can be obtained from the pulse profiles.

We also calculate the limiting case of negligible uncertainties in the knowledge of these angles and of an infinite number of source counts. The uncertainty in the measurement of the neutron-star compactness then becomes

$$\lim_{S \rightarrow \infty} \sigma_u = \left(\frac{\sigma_B}{B}\right) \left(\frac{B}{S}\right) \frac{|\sin i \sin \theta| r_1}{(-r_1 \cos i \cos \theta + \sin i \sin \theta + r_1)^2}. \quad (27)$$

Using equation (22) and after some rearranging of terms, we reach the final result for the limiting case

$$\lim_{S \rightarrow \infty} \frac{\sigma_u}{u} = \left(\frac{\sigma_B}{B}\right) \left(\frac{B}{S}\right) (1-u) \left[1 - \left(1 - \frac{1}{u}\right) \cos i \cos \theta\right]. \quad (28)$$

This expression demonstrates that, even in the case of perfect prior knowledge of the geometry of the system and of an infinite number of accumulated photons, the accuracy in the fractional measurement of the neutron star compactness is proportional to the uncertainty in our measurement of the background (σ_B/B) and to the ratio of the background-to-source counts (B/S).

3.2. Utilizing Additional Constraints

In the previous section, we considered the case of minimal information that can be obtained from the pulse profiles, assuming isotropic emission, slow rotation, and no distance or mass information for the pulsar. We now discuss the additional constraints that can be achieved on the neutron star radius and compactness, if any of these assumptions is relaxed.

We first explore the more favorable case when the emission is anisotropic, i.e., $h \neq 0$. This is also a more realistic consideration because of the strong temperature gradients in the bombarded atmospheres of the polar cap regions. The uncertainties discussed in the previous section all improve because of the presence of one additional constraint related to the measurement of the second harmonic of the profile. The two independently measurable quantities then become

$$\begin{aligned} \frac{V_1}{Q} &= \frac{(1+2hq)v}{q+h(q^2+v^2/2)} \\ \frac{V_2}{Q} &= \frac{hv^2}{2[q+h(q^2+v^2/2)]}. \end{aligned} \quad (29)$$

These two independent pieces of information allow for a unique determination of the auxiliary quantities q and v , which can be used to determine the compactness u and the combination of the angles i and θ (since these angles enter q and v only as a product of their sines and cosines, see eq.[19]). The fractional uncertainties σ_Q/Q and σ_V/V , then, will give rise to similar uncertainties in the two ratios in equation (29). Individually, these translate into uncertainties in the compactness u in much the same way as in the previous section, following Equations (22)-(26). However, combining them allows for smaller uncertainties on the compactness u and the combination of the angles i and θ . More harmonics can be measured also in the case of a moderately spinning star where Doppler effects are detectable (e.g., Psaltis & Özel 2014), leading to similar tightening of the uncertainties.

A similar situation arises when the polar-cap size dS and the measured intensity of radiation I_o are measured spectroscopically and the distance to the source D is known a priori. This is achievable for some of the representative NICER targets where a precise measurement of the distance is possible via pulsar timing parallax or very long baseline interferometry (e.g., PSR J0437–4715, see Deller et al. 2008; Verbiest et al. 2008). In this case, instead of taking the ratios of the various amplitudes, it becomes possible to directly invert equations (20) to obtain the auxiliary quantities u and v . As before, these additional constraints lead to much tighter constraints on the compactness u and the combination of the angles i and θ . The independent knowledge of one of these angles then completely solves the system of equations.

Finally, we consider in Figure 5 the case where the mass of the pulsar is known through other means, such as a dynamical measurement of the pulsar mass in a binary system. This is indeed a likely situation, as a large fraction of millisecond pulsars are in binary systems with white dwarf companions. Currently, there are 17 millisecond pulsars with precisely measured masses, including some of the NICER targets, and this number is growing rapidly (see a recent compilation in Özel & Freire 2016). This figure shows that combining the measurement of the compactness u with a prior knowledge of the mass with an uncertainty that is comparable to that of PSR J0437–4715 ($M = 1.44(7) M_\odot$; Reardon et al. 2016) is sufficient to distinguish between different equations of state.

4. CONCLUSIONS

In this paper, we investigated the effect of instrument or sky background on the determination of neutron star compactness and radius from a measurement of the shapes of pulse profiles from rotation-powered pulsars. Specifically, we made use of analytic formulae for the pulse shapes of moderately spinning neutron stars in the Schwarzschild metric to connect the observables from the profile to the properties of the neutron star. We showed that, in the case of isotropic emission and not utilizing any distance or mass information for the pulsar, the ratio of harmonics can be used to constrain the neutron star compactness. Furthermore, we showed that knowledge of the background at a few percent level for a background-to-source count rate ratio of 0.2 and a total accumulation of 10^6 counts allow

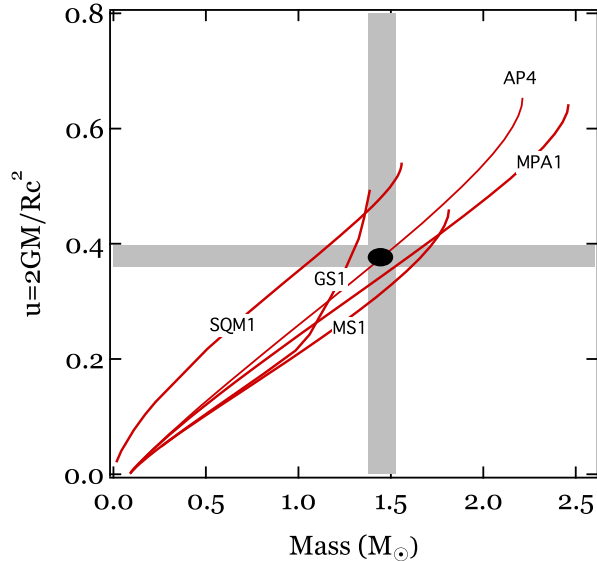


FIG. 5.— The solid curves show the neutron-star compactness as a function of its mass, for a number of representative equations of state. The vertical shaded band represents a dynamical measurement of the mass of a $1.45M_{\odot}$ neutron star with a 5% uncertainty. The horizontal shaded band represents a measurement of its compactness via pulse-profile modeling, with a 5% uncertainty. Achieving such an accuracy is sufficient to distinguish between different equations of state.

for a measurement of the neutron star compactness to better than 10% uncertainty for most of the parameter space. These uncertainties become even smaller for more favorable geometries where the harmonic amplitudes are higher, as is the case for prototypical NICER targets such as PSR J0437–4715. For these geometries, a $\lesssim 6\%$ uncertainty in the compactness is achievable even when the background-to-signal ratio becomes comparable to $B/S \approx 2$ (this is, e.g., a factor of two worse than what is expected for PSR J0030+0451).

Polar caps of rotation powered pulsars emit thermally in the soft X-rays because they are heated from above by particle bombardment from the magnetosphere. In this case, it is expected from model atmosphere calculations that the emission from the surface will be beamed. This anisotropy allows for more fractional harmonic amplitudes to be measured compared to the isotropic case and can reduce the uncertainty in the compactness even further for the same requirements on the background. Similarly, utilizing distance information to the pulsar, when it is known precisely, and when the instrument’s effective area is sufficiently well calibrated, allows for a measurement of the absolute, rather than fractional, amplitudes, increasing the number of directly and independently determined observables to two or three, depending on the beaming of emission. Finally, a mass measurement for the pulsar obtained through pulsar timing enables a precise measurement of the neutron star radius when combined with the compactness measured from the pulse profile. All of these will lead to a more accurate determination of the dense matter equation of state through means that are different from the earlier spectroscopic measurements (see Özel et al. 2015).

REFERENCES

- Abdo, A. A., Ajello, M., Allafort, A., et al. 2013, *ApJS*, 208, 17
Arons, J. 1981, *ApJ*, 248, 1099
Arzoumanian, Z., Gendreau, K. C., Baker, C. L., et al. 2014, *Proc. SPIE*, 9144, 914420
Bai, X., & Spitkovsky, A. 2010a, *ApJ*, 715, 1270
Bai, X., & Spitkovsky, A. 2010b, *ApJ*, 715, 1282
Bauböck, M., Psaltis, D., Özel, F. 2015, *ApJ*, 811, 144
Becker, W., & Trümper, J. 1993, *Nature*, 365, 528
Bogdanov, S., & Grindlay, J. E. 2009, *ApJ*, 703, 1557
Bogdanov, S., Rybicki, G. B., & Grindlay, J. E. 2007, *ApJ*, 670, 668
Braje, T. M., Romani, R. W., & Rauch, K. P. 2000, *ApJ*, 531, 447
Cadeau, C., Morsink, S. M., Leahy, D., & Campbell, S. S. 2007, *ApJ*, 654, 458
Dai, S., Hobbs, G., Manchester, R. N., et al. 2015, *MNRAS*, 449, 3223
Deller, A. T., Verbiest, J. P. W., Tingay, S. J., & Bailes, M. 2008, *ApJ*, 685, L67
Finley, J. P., Ogelman, H., & Kiziloglu, U. 1992, *ApJ*, 394, L21
Gendreau, K. C., Arzoumanian, Z., & Okajima, T. 2012, *Proc. SPIE*, 8443, 844313
Harding, A., & Muslimov, A. 2001, *ApJ*, 556, 987
Harding, A., & Muslimov, A. 2002, *ApJ*, 568, 862
Johnson, T. J., Venter, C., Harding, A. K., et al. 2014, *ApJS*, 213, 6
Morsink, S. M., Leahy, D. A., Cadeau, C., & Braga, J. 2007, *ApJ*, 663, 1244
Nath, N. R., Strohmayer, T. E., & Swank, J. H. 2002, *ApJ*, 564, 353
Ögelman, H. 1991, *NATO Advanced Science Institutes (ASI) Series C*, 344, 87
Özel, F. 2013, *Reports on Progress in Physics*, 76, 016901
Özel, F., & Freire, P. 2016, *ARA&A*, in press
Ozel, F., Psaltis, D., Guver, T., et al. 2015, *ApJ*, in press (arXiv:1505.05155)
Pavlov, G. G., & Zavlin, V. E. 1997, *ApJ*, 490, L91
Pechenick, K. R., Ftaclas, C., & Cohen, J. M. 1983, *ApJ*, 274, 846
Poutanen, J., & Beloborodov, A. M. 2006, *MNRAS*, 373, 836
Psaltis, D., Özel, F. 2014, *ApJ*, 792, 87
Psaltis, D., Özel, F., & Chakrabarty, D. 2014, *ApJ*, 787, 136
Reardon, D. J., Hobbs, G., Coles, W., et al. 2016, *MNRAS*, 455, 1751
Ruderman, M., & Sutherland, P. 1975, *ApJ*, 196, 51
Strohmayer, T. E. 2004, *X-ray Timing 2003: Rossi and Beyond*, 714, 245

Strohmer, T. E., Zhang, W., & Swank, J. H. 1997, *ApJ*, 487, L77
Verbiest, J. P. W., Bailes, M., van Straten, W., et al. 2008, *ApJ*, 679, 675

Weinberg, N., Miller, M. C., & Lamb, D. Q. 2001, *ApJ*, 546, 1098
Yan, W. M., Manchester, R. N., van Straten, W., et al. 2011, *MNRAS*, 414, 2087
Zavlin, V. E. 2006, *ApJ*, 638, 951